Efficient model for field-induced magnetization and magnetostriction of Galfenol

P. G. Evans[a] and M. J. Dapino[b]
Department of Mechanical Engineering, The Ohio State University, Columbus, Ohio 43210, USA

(Received 20 October 2008; accepted 7 April 2009; published online 1 June 2009)

A fully coupled, nonlinear model is presented that characterizes the three-dimensional (3D) strain and magnetization response to magnetic field at constant stress in cubic magnetostrictive materials. A multiscale thermodynamic approach is taken which accounts for nonlinear anisotropy, material texture, and hysteresis effects. The model is validated with measurements of textured polycrystalline Galfenol. The model provides an efficient framework for characterization, design, and control of Galfenol (Fe–Ga) devices with 3D functionality subjected to combined magnetic field and stress loading. © *2009 American Institute of Physics*. [DOI: 10.1063/1.3129316]

I. INTRODUCTION

The direct magnetomechanical effect is the dimensional change associated with a change in magnetic state in magnetic materials. With the advent of magnetostrictive Galfenol, which has ductility similar to steel and can be utilized in three-dimensional (3D) systems, models that predict 3D magnetomechanical behavior have become increasingly important. Magnetic anisotropy and material texture cause the magnetization and strain response to magnetic fields and stresses to depend on the application direction. Magnetostrictive devices have often been limited to unidirectional loading, due in part to the brittleness of Terfenol-D. Accurate, nonlinear, and low-order transducer models often rely on one-dimensional (1D) constitutive models such as the Jiles-Atherton theory of ferromagnetic hysteresis[1] and the Preisach model.[2] Smith's homogenized energy framework[3] is attractive for incorporation into detailed 3D boundary value problems.

Recently, Datta *et al.*[4] presented a 3D, quasistatic transducer model for single-crystal Galfenol in bending which couples Euler–Bernoulli beam theory with the Armstrong[5] model for characterizing magnetomechanical behavior. The 3D Armstrong[5] model has also been used to model the anhysteretic magnetomechanical behavior of polycrystals[6] and hysteresis of single crystals.[7] The model is a statistical approach in which it is assumed that magnetic moment orientations (ϕ, θ) follow a Boltzmann distribution. Magnetomechanical coupling is incorporated through a stress-induced anisotropy term in the total energy (E) used in the distribution. In the Armstrong model, a bulk quantity is calculated as an energy weighted integral of the point-wise quantity over all possible domain orientations,

$$\bar{Q} = \frac{\int_0^{\pi}\int_0^{2\pi} Q(\phi,\theta) e^{-E(\phi,\theta)/\Omega} d\theta d\phi}{\int_0^{\pi}\int_0^{2\pi} e^{-E(\phi,\theta)/\Omega} d\theta d\phi}. \quad (1)$$

The weighted average (1) serves to smooth the sharp transitions obtained by direct minimization of the total energy.

To characterize, design, and control general Galfenol devices with 3D functionality, it is necessary to quantify the effects of domain wall motion, material texture, hysteresis, and transducer geometry. Extending the Armstrong model (1) to include these effects comes at great computational expense, hence limiting the utility of the resulting model. For example, to include irreversible domain wall motion Atulasimha *et al.*[7] approximate the double integral in Eq. (1) with a summation of 98 point evaluations, which leads to 98 ordinary differential equations to be solved. Armstrong's approach to including irreversible domain wall motion is less computationally intensive, as it only considers eight domain orientations corresponding to the eight easy crystal directions or internal energy minima in Terfenol-D.[8] However, the approach is accurate only when the applied field or stress is aligned with an easy crystal axis, since the easy crystal directions do not rotate.

Extending Eq. (1) to include texture effects (neglecting grain boundary interactions) can be done through a summation of double integrals.[6] To solve the boundary-value problem of general Galfenol transducers it is necessary to couple Maxwell's equations with momentum conservation equations through a constitutive model relating magnetization and strain to stress and magnetic field. This system of partial differential equations must be discretized for numerical solution and the constitutive model evaluated at each node. A computationally efficient constitutive model is thus highly desirable.

In this paper we present a low-order constitutive model describing 3D magnetization and 3D strain as a function of applied magnetic field and stress. Owing to its computational efficiency, the model is ideal for design and control of cubic magnetostrictive devices. The model provides greater accu-

[a]Electronic mail: evans.895@osu.edu.
[b]Author to whom correspondence should be addressed. Electronic mail: dapino.1@osu.edu.

racy than Armstrong's[8] hysteresis model, while avoiding the computational expense of the approach presented by Atulasimha *et al.*[7] Rather than discretize Eq. (1) with a large number of fixed orientations, we directly minimize the enthalpy in order to find the stress and magnetic field dependent local minima. Since the empirical smoothing operator (1) most heavily weights the enthalpy minima, good accuracy is achieved using only six orientations which rotate with stress and field.

II. MODEL DEVELOPMENT

Ferromagnetic materials are composed of regions of uniform magnetization M_s called domains.[9] In the Stoner–Wohlfarth (SW) approximation used here and in other magnetomechanical models,[10] the material is modeled as a collection of noninteracting, single-domain particles.[11] The internal energy of a particle is due to magnetocrystalline anisotropy which, for body-centered cubic materials such as Galfenol, makes domains align in the ⟨100⟩ and ⟨111⟩ directions in the absence of field and stress. Work is required to rotate domains away from these easy directions. Gallium content affects the anisotropy energy and hence which directions are easy. Measurements of Galfenol's anisotropy[12] indicate that for Galfenol having less than 20 at. % Ga, the ⟨100⟩ directions are easy. As magnetic fields $\mathbf{H}$ and stresses $\mathbf{T}$ are applied, domains rotate toward the field direction and perpendicular to the principal stress directions. When magnetic domains rotate, the magnetomechanical coupling induces lattice strain and bulk magnetostriction. For a material composed of a collection of SW particles in thermodynamic equilibrium having r possible orientations, the bulk magnetization $\mathbf{M}$ and strain $\mathbf{S}$ due to magnetostriction are the sum of the magnetization $M_s\hat{\mathbf{m}}^k$ and magnetostriction $\hat{\mathbf{S}}_m^k$ due to each orientation, weighted by the volume fraction $\hat{\xi}^k$ of particles in each orientation

$$\mathbf{M} = M_s \sum_{k=1}^{r} \hat{\xi}^k \hat{\mathbf{m}}^k, \quad \mathbf{S} = \sum_{k=1}^{r} \hat{\xi}^k \hat{\mathbf{S}}_m^k. \tag{2}$$

The equilibrium orientations and magnetostrictions are found from the enthalpy of a single SW particle and the equilibrium volume fractions are calculated with the empirical smoothing function (1).

A. Equilibrium orientations

The energy formulation here pertains to noninteracting, single-domain particles in accordance with the SW model for magnetization.[11] The material is assumed to be well below the Curie temperature so that the thermal energy may be neglected. The internal energy of a particle with orientation $\mathbf{m}=[m_1 \;\; m_2 \;\; m_3]$ is due to the magnetocrystalline anisotropy energy, which can be expressed as a series expansion.[9] After considering the cubic crystal symmetry and neglecting higher order terms, the internal energy with natural dependence on magnetization is

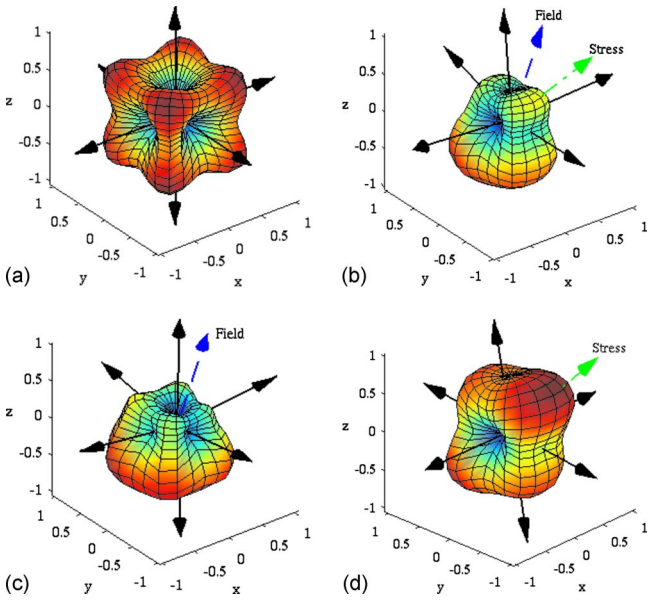

FIG. 1. (Color online) Enthalpy with equilibrium orientations (solid) for (a) no field or stress, (b) field (dash) and stress (dash-dot), (c) field only, (d) and stress only.

$$U(\mathbf{m}) = K_4(m_1m_2 + m_2m_3 + m_3m_1), \tag{3}$$

where K_4 is the fourth-order cubic anisotropy coefficient. The enthalpy is

$$\mathcal{H}(\mathbf{H},\mathbf{T}) = U(\mathbf{m}) - \mathbf{S}_m \cdot \mathbf{T} - \mu_0 M_s \mathbf{m} \cdot \mathbf{H}. \tag{4}$$

Here, $\mathbf{T}$ is the six-element stress vector in which the first three components are the longitudinal stresses and the last three are the shear stresses. The magnetostriction $\mathbf{S}_m = \mathbf{S}_m(\mathbf{m})$ has longitudinal components

$$S_{m,i} = \frac{3}{2}\lambda_{100} m_i^2, \quad i = 1,2,3 \tag{5}$$

and shear components

$$S_{m,4} = 3\lambda_{111} m_1 m_2,$$

$$S_{m,5} = 3\lambda_{111} m_2 m_3,$$

$$S_{m,6} = 3\lambda_{111} m_3 m_1. \tag{6}$$

These expressions are derived by balancing the elastic and magnetoelastic coupling energies.[9]

For $K_4 > 0$, the internal energy has six minima or easy axes ($r=6$) in the ⟨100⟩ directions and for $K_4 < 0$, the internal energy has eight minima or easy axes ($r=8$) in the ⟨111⟩ directions. Applied magnetic and magnetomechanical work rotates particles away from the easy axes toward the magnetic field direction and perpendicular to the principal stress directions (see Fig. 1). The equilibrium orientations ($\hat{\mathbf{m}}_k$; $k=1,\ldots,r$), needed for calculation of the bulk magnetization (2), are obtained through the conditions $\partial\mathcal{H}/\partial m_i = 0$ constrained to a unit sphere. The equilibrium magnetostrictions ($\hat{\mathbf{S}}_m^k$; $k=1,\ldots,r$), needed for calculation of the bulk strain (2) due to magnetostriction, are obtained by evaluating relations (5) and (6) using the equilibrium orientations $\hat{\mathbf{S}}_m^k = \mathbf{S}_m(\hat{\mathbf{m}}^k)$.

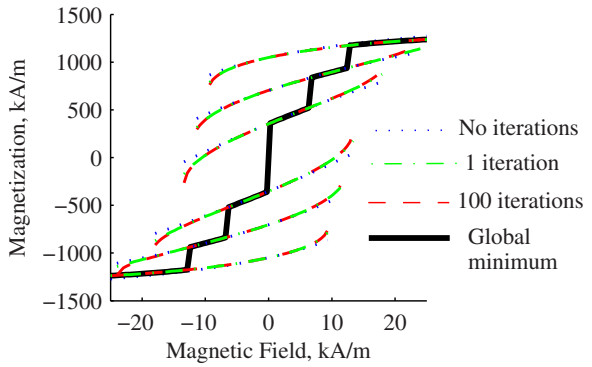

FIG. 2. (Color online) Equilibrium domain orientations for field and stress applied in the [132] direction, calculated with 0, 1, and 100 iterations as described in Sec. II B.

B. Numerical calculation of equilibrium orientations

The derivatives of the enthalpy $\partial\mathcal{H}/\partial m_i$ restricted to a unit sphere are nonlinear functions of m_i yielding equations $\partial\mathcal{H}/\partial m_i=0$ which cannot be solved analytically. Newton's method may be used for approximating a solution. For example, to calculate the energy equilibrium near the [001] easy direction (when $K_4>0$), the system

$$m_3=\sqrt{1-m_1^2-m_2^2}, \tag{7}$$

$$\frac{\partial\mathcal{H}}{\partial m_1}=0, \tag{8}$$

$$\frac{\partial\mathcal{H}}{\partial m_2}=0, \tag{9}$$

is approximately solved by finding the perturbations $\tilde{m}_1$, $\tilde{m}_2$, and $\tilde{m}_3$ about the [001] direction from the linearized system

$$m_3\approx(m_3)_0+\left(\frac{\partial m_3}{\partial m_1}\right)_0\tilde{m}_1+\left(\frac{\partial m_3}{\partial m_2}\right)_0\tilde{m}_2, \tag{10}$$

$$\frac{\partial\mathcal{H}}{\partial m_1}\approx\left(\frac{\partial\mathcal{H}}{\partial m_1}\right)_0+\left(\frac{\partial^2\mathcal{H}}{\partial m_1^2}\right)_0\tilde{m}_1+\left(\frac{\partial^2\mathcal{H}}{\partial m_1 m_2}\right)_0\tilde{m}_2=0, \tag{11}$$

$$\frac{\partial\mathcal{H}}{\partial m_2}\approx\left(\frac{\partial\mathcal{H}}{\partial m_2}\right)_0+\left(\frac{\partial^2\mathcal{H}}{\partial m_1 m_2}\right)_0\tilde{m}_1+\left(\frac{\partial^2\mathcal{H}}{\partial m_2^2}\right)_0\tilde{m}_2=0, \tag{12}$$

where the subscript 0 denotes evaluation of the quantity at the linearization point $(m_1)_0$, $(m_2)_0$, and $(m_3)_0$ which is initially $(m_1)_0=(m_2)_0=0$, and $(m_3)_0=1$ for this case. Greater accuracy is achieved by iterating according to Newton's method. Because of the moderate magnetocrystalline anisotropy of Galfenol, the equilibrium direction will remain near the ⟨100⟩ crystal directions; thus, high accuracy is achieved with few iterations. Figure 2 shows the calculated equilibria with no iteration (linear approximation), 1 iteration, and 100 iterations. Excellent accuracy is achieved with only the linear approximation. The error gets larger as the equilibrium gets further away from the easy crystal direction, i.e., at the ends of the magnetization kernel branches. However, the energy also increases, so the global minimum switches before significant error occurs.

The volume fractions are calculated as the energy weighted average

$$\hat{\xi}^k=\frac{\exp(-\mathcal{H}^k/\Omega)}{\sum_{j=1}^{r}\exp(-\mathcal{H}^j/\Omega)}, \tag{13}$$

where $\mathcal{H}^k$ is the enthalpy of the equilibrium orientation $\mathbf{m}^k$. Substitution of Eq. (13) into Eq. (2) gives the bulk magnetization and magnetostriction

$$\mathbf{M}=\frac{\sum_{k=1}^{r}M_s\hat{\mathbf{m}}^k\exp(-\mathcal{H}^k/\Omega)}{\sum_{k=1}^{r}\exp(-\mathcal{H}^k/\Omega)},\quad \mathbf{S}=\frac{\sum_{k=1}^{r}\hat{\mathbf{S}}^k\exp(-\mathcal{H}^k/\Omega)}{\sum_{k=1}^{r}\exp(-\mathcal{H}^k\Omega)}. \tag{14}$$

The volume fraction ξ^k calculated with Eq. (13) approaches unity as $\mathcal{H}^k$ becomes much less than all other orientation enthalpies $\mathcal{H}^j$. This property makes Eq. (14) a good approximation to Eq. (1) since it considers only orientations which are locally minimum.

C. Single crystal, anhysteretic simulation and discussion

Simulations of anhysteretic, single-crystal behavior in the [001] and [011] directions are shown in Figs. 3 and 4, respectively. The ⟨100⟩ directions are important because Galfenol rods are typically grown with this orientation along the rod axis. The ⟨110⟩ directions are important because thin films manufactured by electrochemical deposition typically have this orientation.[13] The macroscopic magnetization and magnetostriction were calculated from Eq. (14) with $r=6$ which assumes $K_4>0$. Because of the crystal symmetry, both application directions have only three distinct contributions to the macroscopic behavior from the six equilibrium domain orientations. For [001] application there are equilibria which remain fixed in the [001] and [00$\bar{1}$] directions. They are constant with field because they are parallel with the field. A third contribution comes from domains which are aligned with the [100], [$\bar{1}$00], [010], and [0$\bar{1}$0] easy crystal directions in the absence of field and rotate into the direction of the applied field. Application of compressive stress decreases the slope of this contribution and increases its volume fraction. Both of these effects are due to the energy decrease in orientations perpendicular to compressive stress. The volume fraction increase results in a significant increase in macroscopic magnetostriction because more domains go through a full 90° rotation. A kink in the field-magnetization and field-magnetostriction behavior also results as the field eventually pulls all the domains to the [001] direction for positive field and [00$\bar{1}$] direction for negative field.

The [011] application direction differs from the [001] direction in its saturation behavior and magnetostriction magnitude. The domain orientations which contribute to the positive saturation behavior are the domain families which start in the [010] and [001] easy crystal directions, the easy

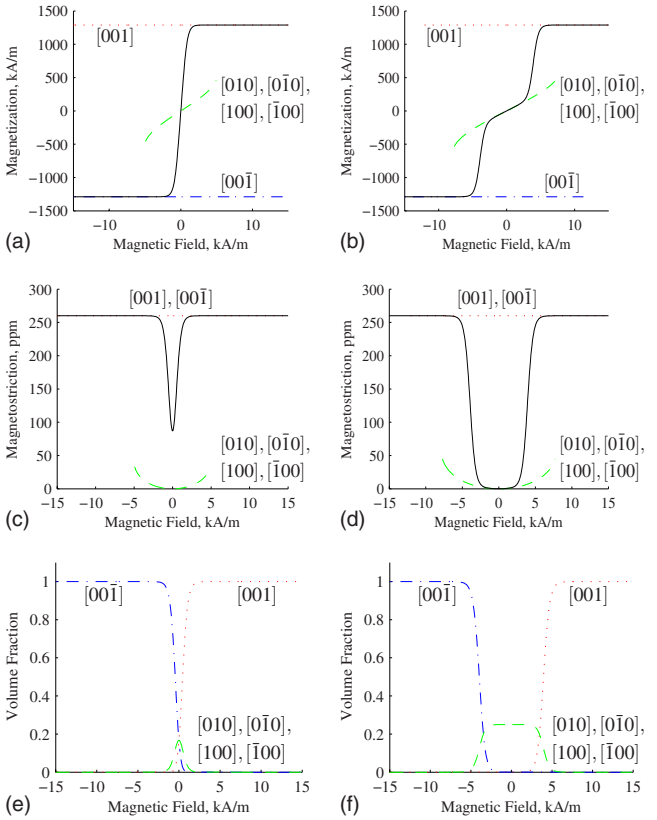

FIG. 3. (Color online) Simulation of the [(a) and (b)] magnetization, [(c) and (d)] magnetostriction, and [(e) and (f)] domain volume fractions for [001] applied field with [(a), (c), and (e)] no prestress and [(b), (d), and (f)] 30 MPa prestress (compression). Solid lines are bulk quantities calculated from Eq. (14) and dashed/dotted lines correspond to local equilibria calculated as described in Sec. II B and by Eq. (13).

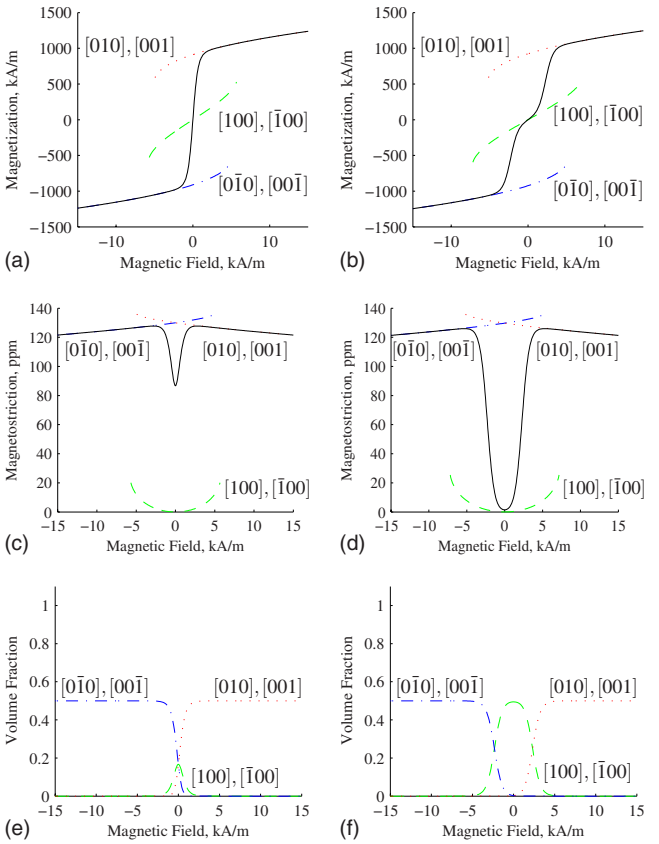

FIG. 4. (Color online) Simulation of the [(a) and (b)] magnetization, [(c) and (d)] magnetostriction, and [(e) and (f)] domain volume fractions for [011] applied field with [(a), (c), and (e)] no prestress and [(b), (d), and (f)] 30 MPa prestress (compression). Solid lines are bulk quantities calculated from Eq. (14) and dashed/dotted lines correspond to local equilibria calculated as described in Sec. II B and by Eq. (13).

crystal directions nearest the positive field direction, and rotate into the applied field direction. The domain orientations which contribute to the negative saturation behavior are the domain families which start in the $[0\bar{1}0]$ and $[00\bar{1}]$ easy crystal directions, the easy crystal directions nearest the negative field direction, and rotate into the applied field direction. Because of this rotation, saturation is gradual rather than abrupt as in the [001] application. Furthermore, the magnetostriction decreases at high fields as the domains rotate away from the easy crystal directions because the material anisotropy is such that the magnetostriction is maximum in the $\langle 100 \rangle$ directions and minimum in the $\langle 111 \rangle$ directions. A third contribution to the macroscopic magnetization and magnetostriction comes from domains which start in the $[100]$ and $[\bar{1}00]$ directions and rotate into the direction of the applied field. Here, also compressive stress decreases the slope of the contribution and increases its volume fraction resulting in an increase in the total magnetostriction.

D. Hysteresis

Armstrong[8] modeled hysteresis due to irreversible domain wall motion by including pinning energy in the evolution of the domain family volume fractions. We take a similar approach,

$$\frac{d\hat{\xi}}{dH} = \frac{\hat{\xi}_{\text{an}} - \hat{\xi}}{K}, \tag{15}$$

where K is proportional to the pinning site energy, $\hat{\xi}_{\text{an}}$ is the anhysteretic volume fraction given by Eq. (13), and H is the magnitude of the applied field. This implementation differs from that of Armstrong in that the domains are allowed to rotate in order to minimize the enthalpy, whereas Armstrong only considered the eight fixed $\langle 111 \rangle$ orientations which correspond to the easy crystal axes or internal energy minima in Terfenol-D. Neglecting domain rotation limits the accuracy of the model, especially when operated in directions away from the easy axes. Atulasimha *et al.*[7] improved the accuracy by considering 98 fixed orientations. Allowing domains to rotate in order to minimize enthalpy is thermodynamically consistent and reduces the number of domain orientations to be tracked to six while preserving accuracy.

This order of magnitude decrease in the number of volume fractions needed for good accuracy is especially important for real-time, model-based controllers and when extending the model to include additional effects such as material geometry and texture. Inclusion of geometry effects necessitates numerical solution of Maxwell's equations, requiring evaluation of the model at many spatial locations. Material texture or polycrystallinity, discussed in the next section, can

be included through stochastic homogenization, which requires many evaluations of the model at each field and stress value.

E. Polycrystallinity

Polycrystallinity is incorporated by considering the material to be composed of regions of uniform crystal lattice having a statistically distributed orientation with respect to the coordinate frame of the applied field and stress. Interactions at the grain boundaries are neglected. This approach is similar to that of Appino *et al.*[14] which considers in-plane domain rotations in polycrystalline materials with uniaxial anisotropy. For 3D rotations with cubic anisotropy, the bulk magnetization takes the form

$$\mathbf{M}_{\text{poly}} = \int_0^{\pi/2} \int_0^{\pi/2} \mathbf{M}(\mathbf{H}, \mathbf{T}, \phi_0, \theta_0) \nu(\phi_0, \theta_0) d\phi_0 d\theta_0, \quad (16)$$

where (ϕ_0, θ_0) is the lattice shift in spherical coordinates of the crystal lattice with respect to the field and stress directions. The grain orientation distribution ν depends on the material texture, which influences the bulk magnetostriction.[15] This approach differs from that of Atulasimha *et al.*[6] in that it considers a continuum of orientations rather than a finite sample and can describe various textures through the density ν. Consider, for example, cylindrical rods grown by the techniques described by Summers *et al.*[16] Orientation imaging microscopy shows a high degree of grain alignment with grains narrowly distributed about the rod axis. This motivates the use of a normal distribution

$$\nu(\phi_0, \theta_0) = \frac{e^{-\phi_0^2/2\sigma^2}}{\sigma\sqrt{2\pi}} \frac{e^{-\theta_0^2/2\sigma^2}}{\sigma\sqrt{2\pi}}, \quad (17)$$

where σ is the standard deviation of the grain misalignment angle. Since the ⟨100⟩ direction has the largest magnetostriction, any off-axis grains tend to decrease the bulk magnetostriction,[16] hence as the distribution broadens (increasing σ), the maximum magnetostriction decreases (see Fig. 5). The degree of grain alignment also affects the kinked shape which arises due to the magnetic and stress anisotropy. Increasing grain misalignment tends to decrease the effect of kinking due to anisotropy (see Fig. 5).

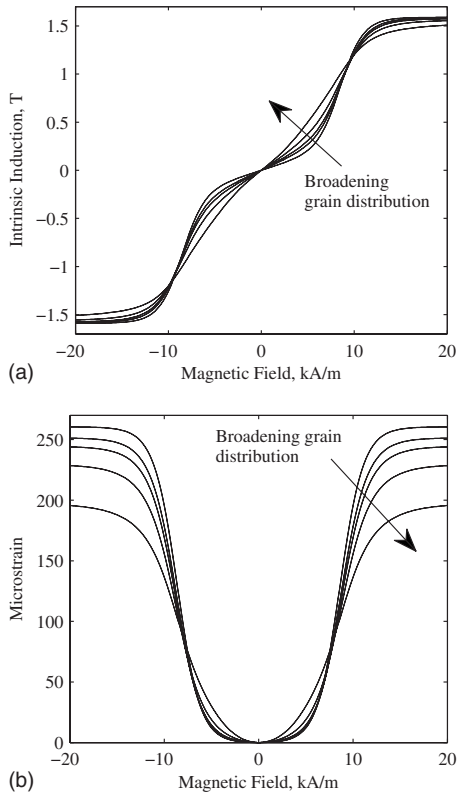

FIG. 5. Inverse effect simulation using Eqs. (16) and (17) with increasing grain misalignment.

III. EXPERIMENTAL VALIDATION

The model given by Eqs. (14)–(16) is validated by comparing simulations to measurements of field-induced magnetization and strain at five levels of constant compressive stress. The integral (16) is computed numerically with Gauss–Quadrature integration and the distribution (17) is used. The material sample used is research grade $Fe_{81.6}Ga_{18.4}$ from Etrema Products Inc., produced by the Free Stand Zone Melt method, which results in a polycrystalline rod with a large percentage of the grains having the [100] direction oriented along the axis of the rod, consistent with Eq. (17). Magnetic field and induction are measured along the rod axis. The model parameters are determined through a least-squares algorithm with initial values in the parameter opti-

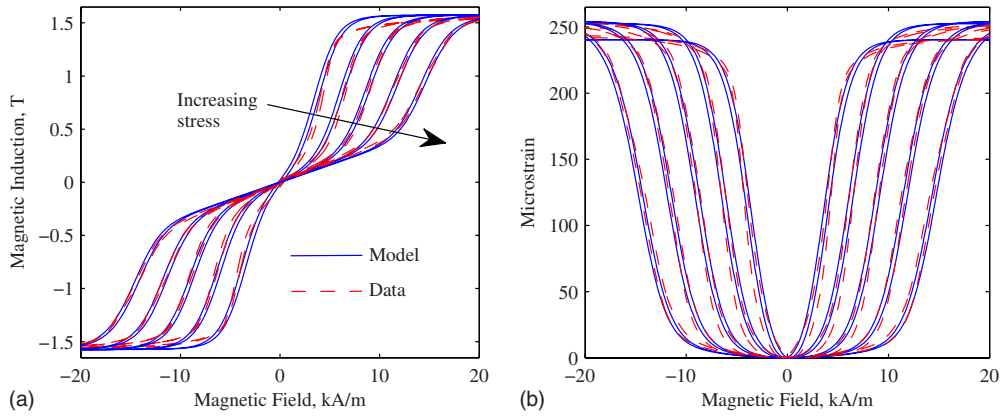

FIG. 6. (Color online) Comparison of Galfenol inverse effect data with the hysteretic, polycrystalline model at stress levels of −13.8, −27.6, −41.4, −55.2, and −69 MPa.

mization algorithm chosen to be consistent with the literature. The optimized parameters are $K=300$ A/m, $\sigma=7.10°$, $M_s=1.26\times10^{-3}$ kA/m, $K_4=36.0$ kJ/m^3, $\lambda_{100}=174$ $\mu\epsilon$, $\lambda_{111}=-13.3$ $\mu\epsilon$, and $\Omega=1.6$ kJ/m^3. The accuracy of the model is illustrated by the fact that a single set of model parameters is used to accurately describe data sets at five different compressive stresses (see Fig. 6).

IV. CONCLUDING REMARKS

A low-order, 3D constitutive model relating magnetization and strain to magnetic field and stress has been developed by utilizing thermodynamic principles with an empirical smoothing operator. By directly minimizing the enthalpy to find the most likely domain orientations, smooth constitutive behavior is achieved with a summation of only six terms. As a result, the framework is extended to include irreversible domain wall motion and material texture without making it too cumbersome for use in distributed parameter, general transducer models which are often solved with the finite-element method, requiring evaluation of the material constitutive model at each node. Comparison of the model to experiments has shown it to accurately model field-induced magnetization and strain at constant stress. The efficiency and accuracy of the model make it ideal for lumped parameter transducer models which may be used for model-based, real-time control of magnetostrictive devices. While accurate, low-order transducer models have been developed for magnetostrictive devices operated in 1D modes, the framework developed here can be used for characterization, design, and control of Galfenol devices capable of 3D magnetic field and stress loading.

ACKNOWLEDGMENTS

We wish to acknowledge the financial support by the Office of Naval Research, MURI Grant No. N000140610530.

[1] M. J. Dapino, R. C. Smith, and A. B. Flatau, IEEE Trans. Magn. **36**, 545 (2000).
[2] X. Tan and J. S. Baras, Automatica **40**, 1469 (2004).
[3] W. S. Oates, P. G. Evans, R. C. Smith, and M. J. Dapino, J. Dyn. Syst., Meas., Control (in press).
[4] S. Datta, J. Atulasimha, and A. B. Flatau, J. Appl. Phys. **101**, 09C521 (2007).
[5] W. D. Armstrong, J. Appl. Phys. **81**, 23217 (1997).
[6] J. Atulasimha, A. B. Flatau, and E. Summers, Smart Mater. Struct. **16**, 1265 (2007).
[7] J. Atulasimha, G. Akhras, and A. B. Flatau, J. Appl. Phys. **103**, 07B336 (2008).
[8] W. D. Armstrong, J. Magn. Magn. Mater. **263**, 208 (2003).
[9] C. Kittel, Rev. Mod. Phys. **21**, 541 (1949).
[10] D. C. Jiles and J. B. Thoelke, J. Magn. Magn. Mater. **134**, 143 (1994).
[11] F. Liorzou, B. Phelps, and D. L. Atherton, IEEE Trans. Magn. **36**, 418 (2000).
[12] S. Rafique, J. R. Cullen, M. Wuttig, and J. Cui, J. Appl. Phys. **95**, 6939 (2004).
[13] R. R. Basantkumar, B. J. Stadler, W. P. Robbins, and E. M. Summers, IEEE Trans. Magn. **42**, 3102 (2006).
[14] C. Appino, M. Valsania, and V. Basso, Physica B **275**, 103 (2000).
[15] R. A. Kellogg, A. Flatau, A. E. Clark, M. Wun-Fogle, and T. Lograsso, J. Intell. Mater. Syst. Struct. **16**, 471 (2005).
[16] E. Summers, T. A. Lograsso, J. D. Snodgrass, and J. Slaughter, Proc. SPIE **5387**, 448 (2004).